

Flat band driven itinerant magnetism in the Co-pnictides (La,Ca)Co₂(As,P)₂

D. Subires,^{1,2,*} M. García-Díez,^{1,3} A. Kar,¹ C.-Y. Lim,¹ Victoria M. Li,⁴ V Yannello,⁵ Dina Carbone,⁶ P. Gargiani,⁷ T. Yilmaz,⁸ J. Dai,⁹ M. Tallarida,⁹ E. Vescovo,⁸ M. Shatruk,⁴ Maia G. Vergniory,^{1,10} and S. Blanco-Canosa^{1,11,†}

¹Donostia International Physics Center (DIPC),

Paseo Manuel de Lardizábal. 20018, San Sebastián, Spain

²Applied Physics Department, University of the Basque Country (UPV/EHU), Basque Country, Bilbao, 48080 Spain

³Physics Department, University of the Basque Country (UPV/EHU), Leioa, Spain

⁴Department of Chemistry and Biochemistry, Florida State University, Tallahassee, Florida 32306, United States

⁵Department of Chemistry and Biochemistry, University of Tampa, 401 W. Kennedy Blvd. Tampa, FL 33606

⁶MAX IV Laboratory, Fotogatan 2, Lund, 225 92, Sweden

⁷ALBA Synchrotron Light Source, Cerdanyola del Vallès, 08290 Barcelona, Catalonia, Spain

⁸National Synchrotron Light Source II, Brookhaven National Laboratory, Upton, New York 11973, USA

⁹ALBA Synchrotron Light Source, 08290 Barcelona, Spain

¹⁰Département de Physique et Institut Quantique,

Université de Sherbrooke, Sherbrooke, J1K 2R1 Québec, Canada.

¹¹IKERBASQUE, Basque Foundation for Science, 48013 Bilbao, Spain

(Dated: March 2025)

Flat bands can induce strong electron correlation effects that help stabilize both magnetic and superconducting states. Here, we carry out angle-resolved photoemission spectroscopy and density functional theory calculations to study the electronic structure of the Co-pnictides CaCo₂As₂ and LaCo₂P₂. We find that, while the k_z Fermi topology of ferromagnetic LaCo₂P₂ is markedly 2-dimensional, antiferromagnetic CaCo₂As₂ develops a 3D Fermi surface described by a *zig-zag*-like band dispersion perpendicular to the Co-As plane. Furthermore, the magnetism is driven by the electronic correlations of the flat bands with d_{xy} and d_{z^2} orbital character at the Fermi level. Our results link the electronic dimensionality and the magnetic order, and emphasize the critical role of the As-As and P-P bond strength along the c -direction to understand the electronic band structure and the rich phase diagram of transition metal pnictides.

The unique interplay between electron-electron correlations and the high density of states at the Fermi level results in strong interactions that throw off their balance and favor unconventional orders. In the case of weakly dispersive flat bands, Coulomb repulsion dominates over the kinetic energy, giving rise to enhanced correlations especially in 2-dimensional (2D) materials and kagome metals that favor magnetism, fractional quantum Hall states and competing phases such as superconductivity and charge density waves [1–8].

Transition metal pnictides with a tetragonal structure, described by the chemical formula AT_2X_2 (A: alkali metal, alkaline-earth metal, lanthanide; T: transition metal; X: metalloid), have garnered renewed attention since the discovery of superconductivity, charge/spin density waves (CDW/SDW) and nematicity in the Fe-based family, AFe_2As_2 [9, 10], and broken rotational and translational symmetries in the Ni-based pnictides [11, 12]. Notably, the Co-pnictides, ACo_2X_2 , do not develop either CDW or superconducting phases at low temperature, but an intriguing cascade of magnetic phase transitions strongly linked to their electronic structure [13]. Besides, the substitution of the A ions [A= Ca, Sr, La, Nd, Pr, Eu,...] in ACo_2X_2 [14] is accompanied by a variation of the Co_2X_2 interlayer distance and X-X

bond angle, leading to a collapsed tetragonal (cT) structure [15, 16] that modify their electronic structure and magnetic order [17, 18].

Although the Co_2X_2 plane is intrinsically 2D, the dimensionality and magnetic order of Co-pnictides can be tuned by electron counting and pressure. For instance, LaCo₂P₂, with an interlayer P-P distance of 3.16 Å, is an in-plane polarized ferromagnet (FM), with $T_C \simeq 130$ K [19, 20], while CaCo₂As₂ (As-As distance of $\simeq 2.73$ Å) has been reported to develop an A-type antiferromagnetic (AFM) ground state ($T_N = 76$ K) coexisting with FM spin fluctuations within the CoAs layer [21] and a spatial anisotropy due to the magnetic frustration arising from the competing FM and AFM interactions [22]. Magnetic order has been observed in the Sr(Ni_{1-x}Co_x)₂P₂ series [23], underscoring the effect of the c/a ratio and chemical doping on the magnetic and electronic properties of Co-pnictides. Similarly, the cascade of magnetic phase transitions in the (Ca,Sr)Co₂P₂ series is accompanied by a change from itinerant-electron FM to AFM order [18, 24, 25], which uncovers novel forms of collective ground states, such as Weyl fermions [26] and Kondo physics [27]. Indeed, CeCo₂P₂ has been reported to be a topological Kondo lattice compound driven by the flat band induced strong interactions and magnetism [28, 29].

On the other hand, despite the magnetism reported experimentally in Co-pnictides, the link between magnetic correlations and electronic dimensionality has not been hitherto addressed. The microscopic origin of the magnetic orders is particularly appealing, since Density Func-

* david.subires@dipc.org

† sblanco@dipc.org

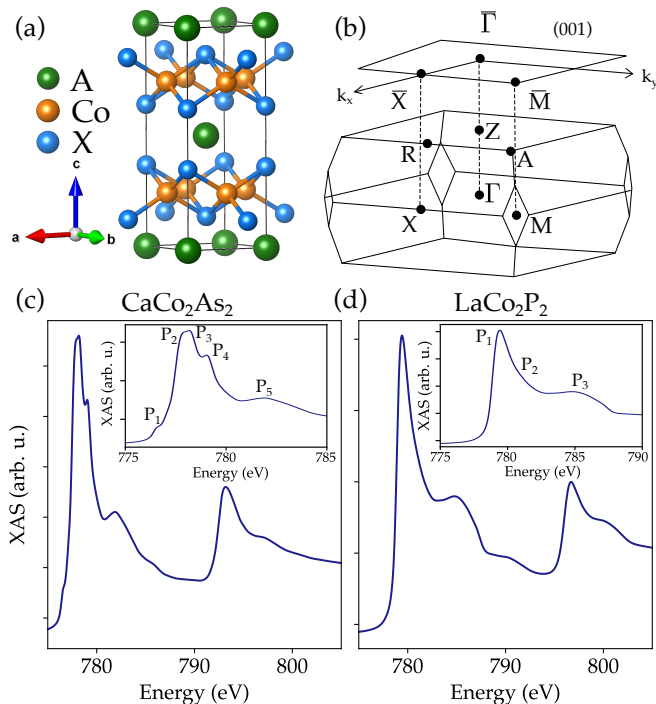


Figure 1. (a) Conventional unit cell of the Co-pnictides with ThCr_2Si_2 -type structure, where $A = \text{Ca, La}$ and $X = \text{As, P}$. (b) Brillouin zone (BZ) and the projected BZ on the (001) surface, along the high symmetry directions. (c-d) Isotropic ($\sigma^+ + \sigma^-$) x-ray absorption spectroscopy (XAS) of CaCo_2As_2 and LaCo_2P_2 , respectively, labeling the different transitions in the inset.

tional Theory (DFT) calculations unveil the presence of a flat band along the Γ -M direction and high density of states (DOS) at the Fermi level. This debate is further stimulated by the observation of flat band induced magnetism in the sibling transition metal dichalcogenide ACo_2Se_2 compound [30, 31] and the coexistence of both AFM and FM spin fluctuations in SrCo_2As_2 [32].

Here, we use angle-resolved photoemission spectroscopy (ARPES) and DFT calculations to accurately describe the orbital contribution of the band structure of AFM and FM Co-pnictides CaCo_2As_2 and LaCo_2P_2 . We find that the electronic structure of CaCo_2As_2 is 3D, in contrast to the 2D observed in the itinerant ferromagnet LaCo_2P_2 . Besides, we demonstrate that the magnetic moment is dominated by the d_{xy} and d_{z^2} orbitals of Co that form a flat band along the Γ -M direction. Our work brings an important piece of information to understand the intertwining of electronic dimensionality and magnetism of a large family of more than 500 layered AT_2X_2 -type compounds.

Single crystals of CaCo_2As_2 and LaCo_2P_2 were grown by Sn-flux method, as previously reported elsewhere [15, 16, 33, 34]. x-ray absorption spectroscopy (XAS) and x-ray magnetic circular dichroism (XMCD) experiments at the Co $L_{2,3}$ -edge were carried out at the BOREAS beamline at the ALBA synchrotron. ARPES

experiments were performed at the BLOCH (MAX IV), ESM (NSLS) and LOREA (ALBA) beamlines, respectively, with experimental energy and angular resolution of 10 meV and 0.1° , respectively. The samples were in-situ cleaved and the measurements were taken at 20 K and above the transition temperatures.

The Co-pnictides $A(\text{Co}(\text{As, P}))_2$ ($A = \text{Ca, La}$) exhibit a body-centered tetragonal ThCr_2Si_2 structure ($I4/mmm$, 139 space group) characterized by alternating stacks of CoX_2 tetrahedral layers (Fig. 1(a)), with the strong bonding within the CoX_2 tetrahedra dominating the interactions, akin to the chemical structure of Fe-pnictides [35]. The conventional unit cell lattice parameters are $a=b=4.01 \text{ \AA}$ and $c_c=10.38 \text{ \AA}$ for CaCo_2As_2 and $a=b=3.80 \text{ \AA}$ and $c_c=11.01 \text{ \AA}$ for LaCo_2P_2 , with the ratio $c_c/a=2.59$ and 2.9, respectively, suggesting a structural link with the magnetic order [16].

Figs. 1 (c-d) display the x-ray absorption (XAS) spectra corresponding to the Co L_3 ($\approx 780 \text{ eV}$) transition that already hints at a different electronic structure. The XAS lineshape strongly depends on the multiplet structure, mainly given by the Co $3d \rightarrow 3d$ and $2p \rightarrow 3d$ Coulomb and exchange interactions, the local crystal fields and the hybridization with the ligands [36]. The absorption edges are separated by $\approx 16 \text{ eV}$ from the L_2 edge ($\sim 795 \text{ eV}$) that result from the spin-orbit split $2p \rightarrow 3d$ transitions. The Co L_3 of CaCo_2As_2 presents five fine structures: a ‘pre-edge’ transition at 776 eV (P_1), a major absorption edge with 2 main peaks at 777.8 eV (P_2) and 778.2 eV (P_3), two high energy shoulders at 779 eV (P_4) and 782 eV (P_5), characteristic of a Co^{2+} oxidation state, see Fig. 1 (c), and a broad absorption line corresponding to the transitions into the continuum above 786 eV. On the other hand, the L_3 structure of LaCo_2P_2 is composed of one main peak (P_1 at 779.4 eV), two shoulders at 781 eV (P_2) and 784.5 eV (P_3), Fig. 1 (d), suggesting a Co oxidation state higher than 2+ (3+ according to the electron counting approach) and the continuum of transitions 10 eV above the main edge [37, 38].

The calculated DOS shows a continuum of metallic states, Fig. 2. In the paramagnetic (PM) calculation, we observe signatures of hybridization between Co and As 4p states, which contributes nearly $\approx 8\%$ to the DOS of CaCo_2As_2 , and the Ca participates with almost $\approx 3\%$ of states in the vicinity of the Fermi level, hence, the total DOS is mainly derived from the Co 3d orbitals that develop a sharp peak at E_F , Fig. 2(a). Interestingly, the sharp peak of the DOS in the PM calculation is split $\pm 0.5 \text{ eV}$ around the Fermi level (Fig. 2(b)), suggesting that electron correlations are responsible for the magnetic order. Similarly, the DOS of LaCo_2P_2 , Fig. 2(f), presents a sharp peak near the Fermi level ($\approx 5 \text{ states/eV}$) in the PM phase, that splits into spin polarized minority and majority bands in the FM phase due to the Stoner mechanism, Fig. 2(g).

In Figs. 2(c) and (h), we show the k_x - k_z Fermi surface of CaCo_2As_2 and LaCo_2P_2 , obtained by varying the incident photon energy from 50 to 120 eV ($\Delta E=2 \text{ eV}$).

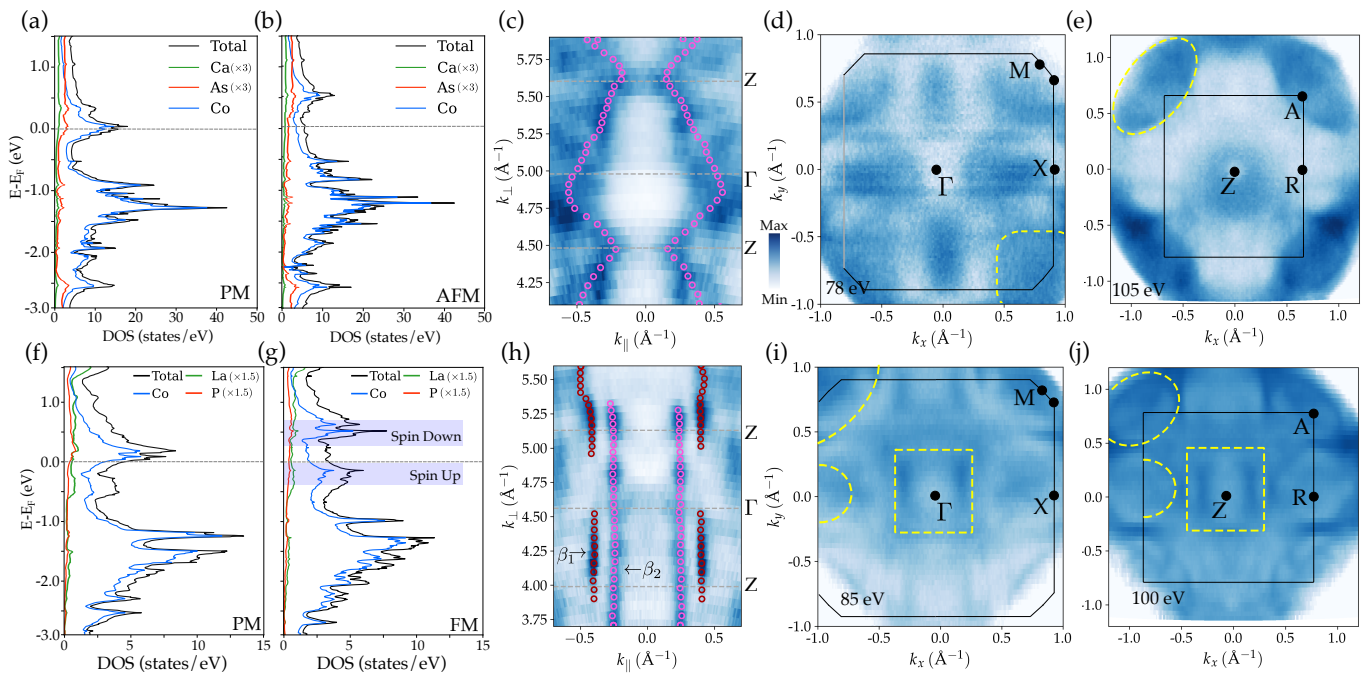


Figure 2. (a-b) Atoms-resolved density of states (DOS) of CaCo_2As_2 for the PM (a) and AFM (b) phases. (c) k_x - k_z Fermi surface of CaCo_2As_2 at $T=20$ K exhibiting a *zig-zag* dispersion along the c -direction, superimposed with the Fermi momenta, (k_f), extracted from the momentum distribution curves (MDCs). (d,e) Fermi surface of CaCo_2As_2 , corresponding to the $k_z = 0$ and $k_z = \frac{\pi}{c}$ planes, taken with $h\nu = 78$ eV and $h\nu = 105$ eV, respectively. (f-g) Total and atoms-resolved DOS for the PM (f) and FM (g) order of LaCo_2P_2 . (h) k_x - k_z Fermi surface of LaCo_2P_2 , $T=20$ K. (i,j) k_x - k_y Fermi surface at the $k_z = 0$ and $k_z = \frac{\pi}{c}$ planes of LaCo_2P_2 , taken with $h\nu = 85$ eV and $h\nu = 100$ eV, respectively, and $T=20$ K. The yellow dashed lines that highlight the electron pockets are a guide to the eye.

The high symmetry points of CaCo_2As_2 , labeled as Γ and Z , are located at 78 and 105 eV, respectively, Fig. 2(d-e). The *zig-zag* dispersion of the bands, superimposed with the Fermi momenta (k_f) obtained from the momentum distribution curves (MDC) of the bands crossing the Fermi level along the c -direction, demonstrates a 3D character of its Fermi surface, 2(c). On the other hand, the k_z dependence of LaCo_2P_2 displays two dispersionless bands, identified as β_1 and β_2 in Fig. 2(h), revealing a pronounced 2-dimensionality of its electronic structure, consistent with the high magnetic field transport data reported in the literature [39].

Figures 2(d-e) and 2(i-j) display the low temperature k_x - k_y Fermi surface (FS) of CaCo_2As_2 and LaCo_2P_2 at $k_z=0$ and $k_z = \frac{\pi}{c}$ planes, being c the lattice parameter of the primitive unit cell (distance between two Co planes), corresponding to the Γ and Z planes. The constant energy contours of the electronic structure present C_4 rotational symmetry, with a rectangular electron pocket at the BZ center [40, 41] and 4 square electron pockets at the corners, M and A points, as expected from the $I4/mmm$ crystal space group.

Centering our attention on the $k_z=0$ plane of CaCo_2As_2 , Fig. 3 (a-c) displays the electronic energy-momentum band dispersion along the high-symmetry path X - Γ - M and its comparison with the projected orbital character of Co obtained *ab initio* in the param-

agnetic state (150 K). At Γ , there is an electron pocket derived from the d_{xy} orbital that develops more spectral weight with LV polarized light. Along the $X-\Gamma$ path, we observe another electron pocket (α) with d_{xz} character, which is only visible with LH polarized light. In addition to these two electron pockets, our high-temperature valence band (VB) spectra resolve a flat band (FB in Fig. 3(a) and suppl. inf. Fig. S7) along the Γ - M direction, resulting from the hybridization of d_{xy} and d_{z^2} orbitals. The momentum spread of the flat band is responsible for the high DOS at E_F in Fig. 2(a) and contributes with $0.39 \mu_B$ (d_{xy}) and $0.12 \mu_B$ (d_{z^2}) to the total magnetization, as calculated *ab initio*. In the $k_z = \frac{\pi}{c}$ plane, there is an electron pocket centered at Z with d_{xy} orbital character, visible with LH light, Fig. 3(e). Along the high-symmetry $Z-A$ line, we can further resolve 2 highly-dispersive bands with $d_{x^2-y^2}$ and d_{xz} orbital characters that cross E_F at $k_f = 0.4 \text{ \AA}^{-1}$ and 0.65 \AA^{-1} , highlighted with vertical arrows in Fig. 3(e). In addition, the small electron pocket at A is also well reproduced by our DFT calculations. Nevertheless, despite the large agreement between ARPES and DFT, we note a mismatch of 0.2 eV of the broad ‘ \wedge ’ band at ≈ 0.4 eV below the E_F , mostly identified with the d_{xz} , d_{yz} and $d_{x^2-y^2}$ orbitals at both $k_z=0$ and $k_z = \frac{\pi}{c}$ planes. We attribute this discrepancy to the magnetic frustration of CaCo_2As_2 [22] that is not fully captured by our DFT cal-

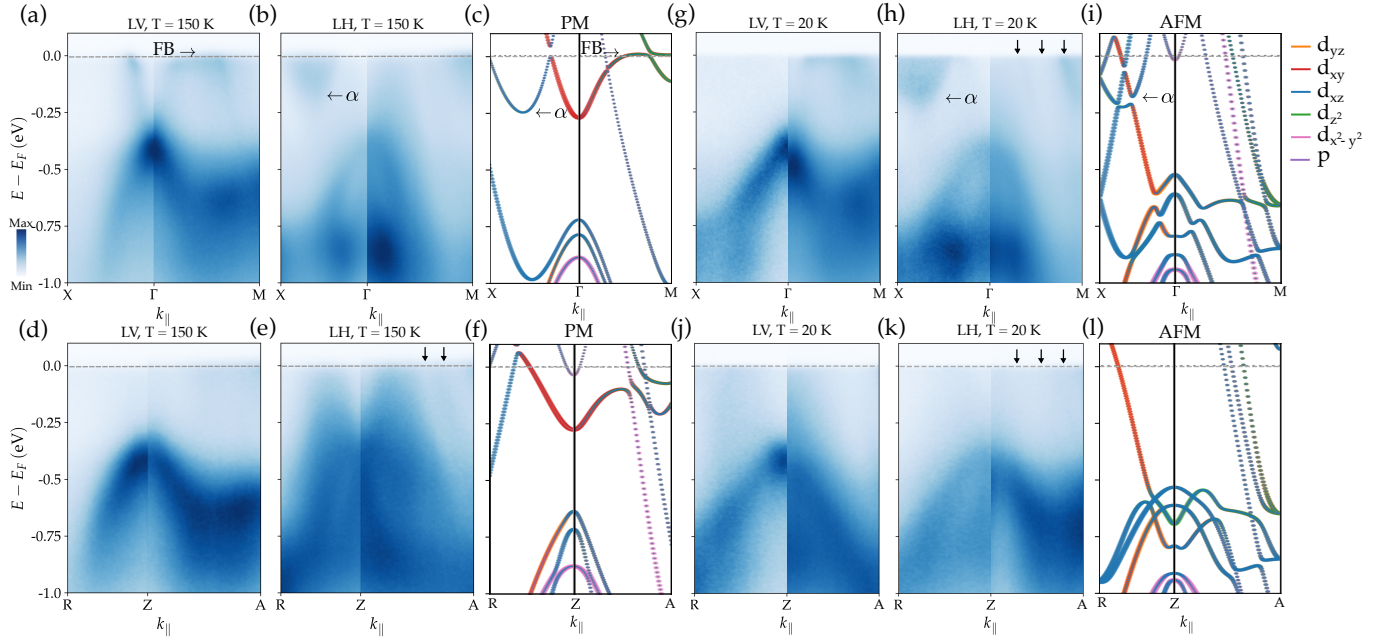


Figure 3. (a-b) Valence band dispersion of CaCo_2As_2 along the high symmetry $X - \Gamma - M$ line at $k_z = 0$ ($E_i = 78$ eV), $T = 150$ K. (c) Orbital resolved DFT calculation of the d orbitals of Co at $k_z = 0$ in the paramagnetic state. (d,e) VB spectrum along the high symmetry $R - Z - A$ line. (f) Atomic-orbital contribution DFT calculation of the d orbitals of Co at $k_z = \frac{\pi}{c}$. (g-h) VB dispersion at low temperature and $k_z = 0$ (i) DFT calculation for $k_z = 0$, and (j-i) for $k_z = \frac{\pi}{c}$. See supp. inf. Fig. 6 for high-resolution VBs that identify the bands crossing the Fermi level in (h) and (k).

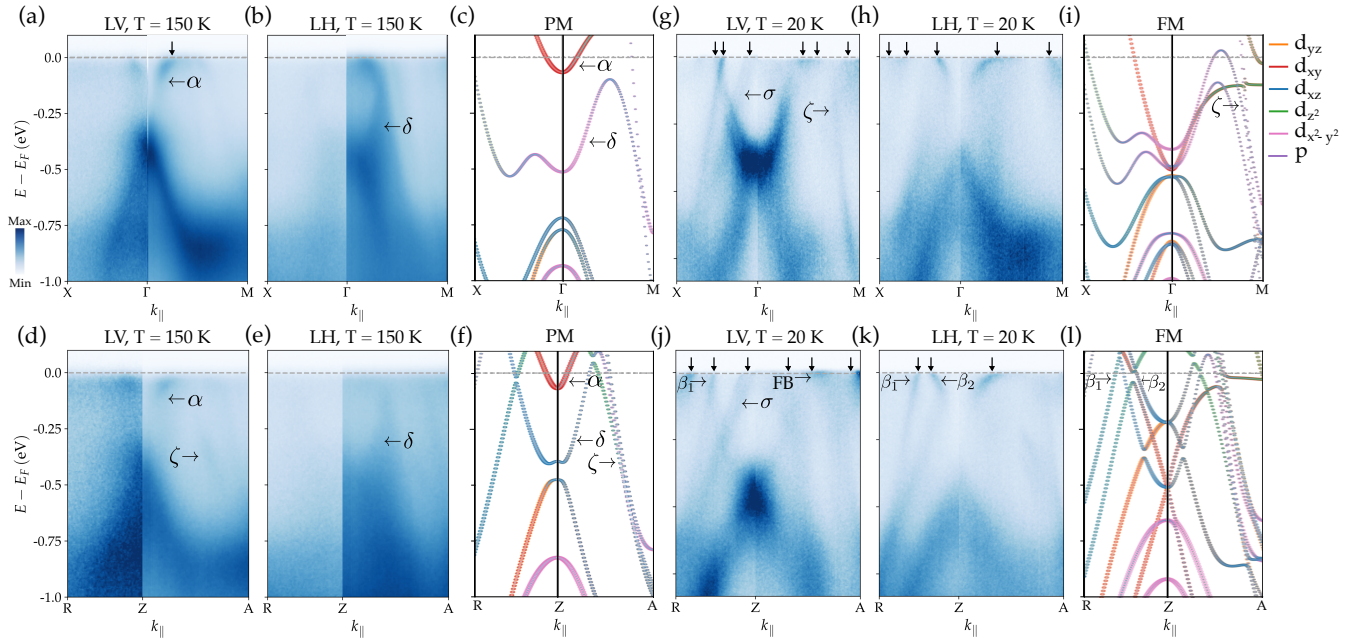


Figure 4. (a-b) VB dispersion along the high symmetry $X - \Gamma - M$ line for LaCo_2P_2 , $k_z = 0$ ($E_i = 85$ eV), $T = 150$ K. (c) Orbital resolved VB at $k_z = 0$. (d,e) Band dispersion following the $R - Z - A$ path, $E_i = 100$ eV. (f) Orbital contribution to the band structure at $k_z = \frac{\pi}{c}$. (g-h) Band dispersion at low temperature, $T = 20$ K and $k_z = 0$ plane. (i) VB DFT calculation at $k_z = 0$. (j-k) Band dispersion and (l) DFT calculation at the $k_z = \frac{\pi}{c}$ plane.

culations. Indeed, the position of the ‘ \wedge ’ band is well reproduced by the FM calculation, see suppl. inf. Fig. S4, further supporting the frustrated square lattice scenario. At low temperature, Fig. 3(g-h), the band structure of CaCo_2As_2 is substantially modified. Notably, the electron pocket at Γ disappears, an electron pocket is visible along the Γ -X path, Fig. 3(h) (d_{xy} and d_{xz} hybridized bands). Besides, along the Γ – M direction, we identify three highly-dispersive bands with Fermi momenta, $k_f = 0.3 \text{ \AA}^{-1}$, 0.6 \AA^{-1} and 0.8 \AA^{-1} , marked by arrows in Fig. 3(h) (see suppl. inf. Fig. S5, for higher resolution VBs), also well reproduced by the AFM DFT calculations in Fig. 3(i). In the $k_z = \frac{\pi}{c}$ plane, the bands along the Z – A path have Fermi momenta $k_f = 0.25 \text{ \AA}^{-1}$, 0.6 \AA^{-1} and 0.8 \AA^{-1} , similar to the highly-dispersive bands in the $k_z = 0$ plane. These highly-disperse bands and the ‘ \wedge ’-shaped set of bands 0.4 eV below E_F retain their orbital characters with respect to the high temperature paramagnetic phase, Figs. 3(g-h) and (j-k).

The experimental band structure of the PM (150 K) and FM (20 K) phases of LaCo_2P_2 and the *ab-initio* calculations are plotted in Fig. 4. At high temperature, the ‘ \wedge ’ shaped band shows up at Γ around $\simeq 0.4$ eV below E_F , Fig. 4(a), and its orbital contribution, d_{xz} , and $d_{x^2-y^2}$, is well discerned in the polarization dependent VB spectra. The top of this band approaches the electron pocket (α) and crosses E_F at $k_f = 0.18 \text{ \AA}^{-1}$, vertical arrow in Fig. 4(a), with most of its spectral weight derived from the d_{xy} orbital. In addition, the VBs with LH light show an electron-like band (δ), d_{xz} and $d_{x^2-y^2}$ orbital character, centered at Γ with its bottom at a binding energy of ~ 0.4 eV. In the $k_z = \frac{\pi}{c}$ plane, Fig. 4(d-e), the electronic energy bands show similar features as in the Γ -plane, with the faint electron pocket (α) and electron-like band (δ) centered at Γ . Moreover, two highly linear dispersive bands (ζ), visible for LV polarized light, are shown along the Z – A direction, in agreement with the DFT calculations. At low temperature, Fig. 4(g-l), we resolve a large electron pocket around Γ and $k_z \sim 0$, Fig. 4(g), which presents mostly $d_{x^2-y^2}$ and d_{yz} character. Such electron pocket cuts E_F at $k_f = 0.47 \text{ \AA}^{-1}$ along X – Γ and Γ – M paths, with the dispersive band (ζ) along Γ – M direction derived from the $d_{x^2-y^2}$ orbital, Fig. 4(g). The VBs show linear dispersing bands along the R-Z-A path with different d orbital characters, whose cuts at the E_F are highlighted by arrows in Fig. 4(j) and (k), again well captured by our DFT calculations. Finally, the flat-ish band along the Z-A path, derived also from the d_{xy} and d_{z^2} orbitals of Co, contributes with 0.62 and 0.22 μ_B , respectively, to the total magnetic moment, see suppl. inf. Table I. The detailed electronic structure shows a small contribution of the pnictide orbitals, with the 3*p* electrons of P and the 4*p* electrons of As contributing to the p - d bonding at higher binding energies.

I. DISCUSSION

We have carried out a comprehensive study of the electronic band structure of CaCo_2As_2 and LaCo_2P_2 , both from ARPES and DFT. We have demonstrated that the Fermi surface of CaCo_2As_2 is markedly 3D with dispersive electronic bands in the k_x - k_z plane, but dispersionless in LaCo_2P_2 . Moreover, the experimental Fermi pocket sizes are similar to the DFT predictions, hence indicating that the electronic correlations in $(\text{Ca,L a})\text{Co}_2(\text{As,P})_2$ are weaker than in their sibling iron pnictides. It follows that the dimensionality of the band structure of Co-pnictides is directly linked to the magnetic order and, hence, a consequence of X-X (As-As or P-P) separation between CoX_2 planes. The shorter As-As distance in CaCo_2As_2 ($\simeq 2.80 \text{ \AA}$) favors a strong covalent bond along the c -direction, featuring a cT phase that enhances the magnetic exchange interaction along the c -axis that promotes an AFM order, given that the energy difference between the AFM and FM states in CaCo_2As_2 is rather small. On the other hand, the P-P distance increases by 16% in LaCo_2P_2 , reducing the coupling between the Co-P planes and forcing an FM order, assisted by the strong in-plane magnetic anisotropy of Co atoms.

As sibling compounds of superconducting iron pnictides, CaCo_2As_2 and LaCo_2P_2 present very different band structure. 122 $(\text{Ca,B a})\text{Fe}_2\text{As}_2$ exhibits a second-order-like stripe pattern followed by a first-order structural transition to a cT phase at low temperature that underscores the emergence of a broken rotational symmetry state [9]. From the electronic structure point of view, the iron pnictides have several hole pockets at Γ that nest the electron pockets around M point, driving the AFM order with a propagation vector $(\pi, 0)$. As a direct consequence of adding one more electron from Co, the upward shift of the chemical potential by ~ 1 eV [42] and the presence of electron pockets away from the X position in CaCo_2As_2 prevent the in-plane FS nesting. Interestingly, the ARPES data we report here show parallels to the dimensionality crossover observed in the 122 family. In particular, a 3D k_z dispersion of the electronic band structure develops in the frustrated AFM CaCo_2As_2 , akin to the three dimensional topology crossover observed in the orthorhombic phase at low temperature in 122 CaFe_2As_2 [43], yet the spin polarization changes from out to in-plane. Nevertheless, the cT phase of Fe pnictides is non-magnetic as a consequence of a major topological change of the Fermi surface that reduces the nesting between the Γ and M pockets. Finally, the FM order in LaCo_2P_2 reconstructs the electronic structure and the number of dispersive bands at low temperature. This is attributed to spin splitting caused by the Stoner-driven magnetic ordering, similar to the electronic structure of RbCo_2Se_2 that shares the same lattice structure [44].

In summary, we have presented a comprehensive analysis of the band structure that demonstrate a correlation between magnetic order, chemical pressure and elec-

tronic dimensionality in the 122 Co-pnictides CaCo_2As_2 and LaCo_2P_2 . We have reported a pronounced 2-dimensionality of the electronic structure of LaCo_2P_2 , in contrast to the 3D character of CaCo_2As_2 . The experimental and calculated band structure indicate that Co-pnictides undergo a large Fermi-surface reconstruction at the magnetic transitions, which are a consequence of the flat-*ish* bands of Co. Moreover, we have shown that the shorter As-As compared with P-P distance enhances hopping between pnictogen and transition metal and, hence favors the AFM ordering in CaCo_2As_2 . Our findings deepen in the fundamental understanding of the electronic band structure of a large family of compounds that host a variety of collective ground states and provide evidence that the structural, electronic and magnetic properties are strongly entangled.

II. ACKNOWLEDGEMENTS

D.S., A.K. and S.B.-C. acknowledge financial support from the MINECO of Spain through the project PID2021-122609NB-C21 and by MCIN and by the European Union Next Generation EU/PRTR-C17.I1, as well as by IKUR Strategy under the collaboration agreement between IKERBASQUE Foundation and DIPC on behalf of the Department of Education of the Basque Government. C.-Y.L. was supported by the European

Research Council (ERC) under the European Union's Horizon 2020 research and innovation program (Grant Agreement No. 101020833). M.G.D. acknowledges financial support from Government of the Basque Country through the pre-doctoral fellowship PRE 2023 2 0024. M.S. acknowledges the support from the National Science Foundation (award DMR-2233902). This research used resources of the ESM beamline of the National Synchrotron Light Source II, a U.S. Department of Energy (DOE) Office of Science User Facility operated for the DOE Office of Science by Brookhaven National Laboratory under Contract No. DE-SC0012704. LOREA beamline is co-funded by the European Regional Development Fund (ERDF) within the "Framework of the Smart Growth Operative Programme 2014-2020". We acknowledge the MAX IV Laboratory for beamtime on the Bloch beamline under proposal 20210823. Research conducted at MAX IV, a Swedish national user facility, is supported by Vetenskapsrådet (Swedish Research Council, VR) under contract 2018-07152, Vinnova (Swedish Governmental Agency for Innovation Systems) under contract 2018-04969 and Formas under contract 2019-02496. P.G. acknowledges financial support from the MINECO project PID2023-149494NB-C32. M.G.V. thanks support to the Spanish Ministerio de Ciencia e Innovación (PID2022-142008NB-I00), the Canada Excellence Research Chairs Program for Topological Quantum Matter and the Diputación Foral de Gipuzkoa Programa Mujeres y Ciencia.

-
- [1] F. Wang and H. Zhang, Flat bands and magnetism in Fe_4GeTe_2 and Fe_5GeTe_2 due to bipartite crystal lattices, *Phys. Rev. B* **108**, 195140 (2023).
- [2] J.-X. Yin, S. S. Zhang, G. Chang, Q. Wang, S. S. Tsirkin, Z. Guguchia, B. Lian, H. Zhou, K. Jiang, I. Belopolski, N. Shumiya, D. Multer, M. Litskevich, T. A. Cochran, H. Lin, Z. Wang, T. Neupert, S. Jia, H. Lei, and M. Z. Hasan, Negative flat band magnetism in a spin-orbit-coupled correlated kagome magnet, *Nature Physics* **15**, 443 (2019).
- [3] Z. Ren, J. Huang, H. Tan, A. Biswas, A. Pulkkinen, Y. Zhang, Y. Xie, Z. Yue, L. Chen, F. Xie, K. Allen, H. Wu, Q. Ren, A. Rajapitamahuni, A. K. Kundu, E. Vescovo, J. Kono, E. Morosan, P. Dai, J.-X. Zhu, Q. Si, J. Minár, B. Yan, and M. Yi, Persistent flat band splitting and strong selective band renormalization in a kagome magnet thin film, *Nature Communications* **15**, 9376 (2024).
- [4] X. Qian, J. Liu, L. Fu, and J. Li, Quantum spin hall effect in two-dimensional transition metal dichalcogenides, *Science* **346**, 1344 (2014), <https://www.science.org/doi/pdf/10.1126/science.1256815>.
- [5] R. Bistritzer and A. H. MacDonald, Moiré bands in twisted double-layer graphene, *Proceedings of the National Academy of Sciences* **108**, 12233 (2011), <https://www.pnas.org/doi/pdf/10.1073/pnas.1108174108>.
- [6] J. Herzog-Arbeitman, A. Chew, D. K. Efetov, and B. A. Bernevig, Reentrant correlated insulators in twisted bilayer graphene at 25 t (2π flux), *Phys. Rev. Lett.* **129**, 076401 (2022).
- [7] Z. Lin, J.-H. Choi, Q. Zhang, W. Qin, S. Yi, P. Wang, L. Li, Y. Wang, H. Zhang, Z. Sun, L. Wei, S. Zhang, T. Guo, Q. Lu, J.-H. Cho, C. Zeng, and Z. Zhang, Flatbands and emergent ferromagnetic ordering in Fe_3Sn_2 kagome lattices, *Phys. Rev. Lett.* **121**, 096401 (2018).
- [8] M. Kang, L. Ye, S. Fang, J.-S. You, A. Levitan, M. Han, J. I. Facio, C. Jozwiak, A. Bostwick, E. Rotenberg, M. K. Chan, R. D. McDonald, D. Graf, K. Kaznatcheev, E. Vescovo, D. C. Bell, E. Kaxiras, J. van den Brink, M. Richter, M. Prasad Ghimire, J. G. Checkelsky, and R. Comin, Dirac fermions and flat bands in the ideal kagome metal Fe_3Sn_2 , *Nature Materials* **19**, 163 (2020).
- [9] R. M. Fernandes, A. I. Coldea, H. Ding, I. R. Fisher, P. J. Hirschfeld, and G. Kotliar, Iron pnictides and chalcogenides: a new paradigm for superconductivity, *Nature* **601**, 35 (2022).
- [10] Q. Si, R. Yu, and E. Abrahams, High-temperature superconductivity in iron pnictides and chalcogenides, *Nature Reviews Materials* **1**, 16017 (2016).
- [11] Y. Yao, R. Willa, T. Lacomme, S.-M. Souliou, M. Frachet, K. Willa, M. Merz, F. Weber, C. Meingast, R. Heid, A.-A. Haghighirad, J. Schmalian, and M. Le Tacon, An electronic nematic liquid in BaNi_2As_2 , *Nature Communications* **13**, 4535 (2022).
- [12] Y. Song, S. Wu, X. Chen, Y. He, H. Uchiyama, B. Li, S. Cao, J. Guo, G. Cao, and R. Birgeneau, Phonon soft-

- ening and slowing-down of charge density wave fluctuations in BaNi_2As_2 , *Phys. Rev. B* **107**, L041113 (2023).
- [13] M. Reehuis, W. Jeitschko, G. Kotzyba, B. Zimmer, and X. Hu, Antiferromagnetic order in the ThCr_2Si_2 type phosphides CaCo_2P_2 and CeCo_2P_2 , *Journal of Alloys and Compounds* **266**, 54 (1998).
- [14] M. Imai, C. Michioka, H. Ueda, A. Matsuo, K. Kindo, and K. Yoshimura, Substitution effects in the itinerant electron metamagnetic compound SrCo_2P_2 , *Physics Procedia* **75**, 142 (2015), 20th International Conference on Magnetism, ICM 2015.
- [15] X. Tan, G. Fabbris, D. Haskel, A. A. Yaroslavtsev, H. Cao, C. M. Thompson, K. Kovnir, A. P. Menushenkov, R. V. Chernikov, V. O. Garlea, and M. Shatruk, A transition from localized to strongly correlated electron behavior and mixed valence driven by physical or chemical pressure in ACo_2As_2 ($A = \text{Eu}$ and Ca), *Journal of the American Chemical Society* **138**, 2724 (2016).
- [16] X. Tan, Z. P. Tener, and M. Shatruk, Correlating itinerant magnetism in RCo_2Pn_2 pnictides ($R = \text{La}, \text{Ce}, \text{Pr}, \text{Nd}, \text{Eu}, \text{Ca}$; $\text{Pn} = \text{P}, \text{As}$) to their crystal and electronic structures, *Accounts of Chemical Research* **51**, 230 (2018).
- [17] J. K. Clark, X. Tan, V. O. Garlea, A. A. Arico, A. P. Ramirez, V. Yannello, C. M. Thompson, K. Kovnir, and M. Shatruk, Reentrant spin glass state induced by structural phase transition in $\text{La}_{0.4}\text{Ce}_{0.6}\text{Co}_2\text{P}_2$, *Phys. Rev. Mater.* **4**, 074412 (2020).
- [18] S. Jia, A. J. Williams, P. W. Stephens, and R. J. Cava, Lattice collapse and the magnetic phase diagram of $\text{Sr}_{1-x}\text{Ca}_x\text{Co}_2\text{P}_2$, *Phys. Rev. B* **80**, 165107 (2009).
- [19] M. Reehuis, C. Ritter, R. Ballou, and W. Jeitschko, Ferromagnetism in the ThCr_2Si_2 type phosphide LaCo_2P_2 , *Journal of Magnetism and Magnetic Materials* **138**, 85 (1994).
- [20] W. Zhang, K. Nadeem, H. Xiao, R. Yang, B. Xu, H. Yang, and X. G. Qiu, Spin-flop transition and magnetic phase diagram in CaCo_2As_2 revealed by torque measurements, *Phys. Rev. B* **92**, 144416 (2015).
- [21] B. Cheng, B. F. Hu, R. H. Yuan, T. Dong, A. F. Fang, Z. G. Chen, G. Xu, Y. G. Shi, P. Zheng, J. L. Luo, and N. L. Wang, Field-induced spin-flop transitions in single-crystalline CaCo_2As_2 , *Phys. Rev. B* **85**, 144426 (2012).
- [22] A. Sapkota, B. G. Ueland, V. K. Anand, N. S. Sangeetha, D. L. Abernathy, M. B. Stone, J. L. Niedziela, D. C. Johnston, A. Kreyssig, A. I. Goldman, and R. J. McQueeney, Effective one-dimensional coupling in the highly frustrated square-lattice itinerant magnet CaCo_2As_2 , *Phys. Rev. Lett.* **119**, 147201 (2017).
- [23] J. Schmidt, G. Gorgen-Lesseux, R. A. Ribeiro, S. L. Bud'ko, and P. C. Canfield, Effects of co substitution on the structural and magnetic properties of $\text{Sr}(\text{Ni}_{1-x}\text{Co}_x)_2\text{P}_2$, *Phys. Rev. B* **108**, 174415 (2023).
- [24] J. Sugiyama, H. Nozaki, M. Harada, I. Umegaki, Y. Higuchi, K. Miwa, M. Imai, C. Michioka, K. Yoshimura, E. J. Ansaldo, J. H. Brewer, D. Andreica, C. Baines, and M. Mansson, Magnetic phases in $\text{Sr}_{1-x}\text{Ca}_x\text{Co}_2\text{P}_2$ studied by μ^+ sr, *Physics Procedia* **75**, 426 (2015), 20th International Conference on Magnetism, ICM 2015.
- [25] J. J. Ying, Y. J. Yan, A. F. Wang, Z. J. Xiang, P. Cheng, G. J. Ye, and X. H. Chen, Metamagnetic transition in $\text{Ca}_{1-x}\text{Sr}_x\text{Co}_2\text{As}_2$ ($x = 0$ and 0.1) single crystals, *Phys. Rev. B* **85**, 214414 (2012).
- [26] Y. Xu, L. Elcoro, Z.-D. Song, B. J. Wieder, M. G. Vergniory, N. Regnault, Y. Chen, C. Felser, and B. A. Bernevig, High-throughput calculations of magnetic topological materials, *Nature* **586**, 702 (2020).
- [27] G. Poelchen, I. P. Rusinov, S. Schulz, M. Güttler, M. Mende, A. Generalov, D. Y. Usachov, S. Danzenbächer, J. Hellwig, M. Peters, K. Kliemt, Y. Kucherenko, V. N. Antonov, C. Laubschat, E. V. Chulkov, A. Ernst, K. Kummer, C. Krellner, and D. V. Vyalikh, Interlayer coupling of a two-dimensional kondo lattice with a ferromagnetic surface in the antiferromagnet CeCo_2P_2 , *ACS Nano* **16**, 3573 (2022).
- [28] D. F. Liu, Y. F. Xu, H. Y. Hu, J. Y. Liu, T. P. Ying, Y. Y. Lv, Y. Jiang, C. Chen, Y. H. Yang, D. Pei, D. Prabhakaran, M. H. Gao, J. J. Wang, Q. H. Zhang, F. Q. Meng, B. Thiagarajan, C. Polley, M. Hashimoto, D. H. Lu, N. B. M. Schröter, V. N. Strocov, A. Louat, C. Cao, D. Biswas, T. L. Lee, P. Steadman, P. Bencok, Y. B. Chen, L. Gu, T. Hesjeda, G. van der Laan, H. Hosono, L. X. Yang, Z. K. Liu, H. Q. Yuan, B. A. Bernevig, and Y. L. Chen, Discovery of an antiferromagnetic topological nodal-line kondo semimetal, (2024), [arXiv:2411.13898 \[cond-mat.str-el\]](https://arxiv.org/abs/2411.13898).
- [29] H. Hu, Y. Jiang, D. Liu, Y. Chen, A. M. Tsvetlik, Y. Xu, and B. A. Bernevig, *CeCo2p2: a unique co-antiferromagnetic topological heavy-fermion system with $p \cdot \mathcal{T}$ -protected kondo effect and nodal-line excitations* (2024), [arXiv:2411.13647 \[cond-mat.str-el\]](https://arxiv.org/abs/2411.13647).
- [30] J. Yang, B. Chen, H. Wang, Q. Mao, M. Imai, K. Yoshimura, and M. Fang, Magnetic properties in layered aco_2se_2 ($a = \text{k}, \text{rb}, \text{cs}$) with the thcr_2si_2 -type structure, *Phys. Rev. B* **88**, 064406 (2013).
- [31] J. Huang, Z. Wang, H. Pang, H. Wu, H. Cao, S.-K. Mo, A. Rustagi, A. F. Kemper, M. Wang, M. Yi, and R. J. Birgeneau, Flat-band-induced itinerant ferromagnetism in rbco_2se_2 , *Phys. Rev. B* **103**, 165105 (2021).
- [32] Y. Li, Z. Yin, Z. Liu, W. Wang, Z. Xu, Y. Song, L. Tian, Y. Huang, D. Shen, D. L. Abernathy, J. L. Niedziela, R. A. Ewings, T. G. Perring, D. M. Pajerowski, M. Matsuda, P. Bourges, E. Mechthild, Y. Su, and P. Dai, Coexistence of ferromagnetic and stripe antiferromagnetic spin fluctuations in srco_2as_2 , *Phys. Rev. Lett.* **122**, 117204 (2019).
- [33] M. Shatruk, Thcr_2si_2 structure type: The “perovskite” of intermetallics, *Journal of Solid State Chemistry* **272**, 198 (2019).
- [34] D. K. Mann, A. M. Díez, J. Xu, O. I. Lebedev, Y. V. Kolen'ko, and M. Shatruk, Polar layered intermetallic LaCo_2P_2 as a water oxidation electrocatalyst, *ACS Applied Materials & Interfaces* **14**, 14120 (2022).
- [35] T. C. Ozawa and S. M. Kauzlarich, Chemistry of layered d-metal pnictide oxides and their potential as candidates for new superconductors, *Science and Technology of Advanced Materials* **9**, 033003 (2008).
- [36] M. W. Haverkort, M. Zwierzycki, and O. K. Andersen, Multiplet ligand-field theory using wannier orbitals, *Phys. Rev. B* **85**, 165113 (2012).
- [37] M. W. Haverkort, Z. Hu, J. C. Cezar, T. Burnus, H. Hartmann, M. Reuther, C. Zobel, T. Lorenz, A. Tanaka, N. B. Brookes, H. H. Hsieh, H.-J. Lin, C. T. Chen, and L. H. Tjeng, Spin state transition in laco_3 studied using soft x-ray absorption spectroscopy and magnetic circular dichroism, *Phys. Rev. Lett.* **97**, 176405 (2006).

- [38] A. Ahad, K. Gautam, S. S. Majid, S. Francoual, F. Rahman, F. M. F. De Groot, and D. K. Shukla, Origin of the high seebeck coefficient of the misfit $[\text{ca}_2\text{coo}_3]_{0.62}[\text{coo}_2]$ cobaltate from site-specific valency and spin-state determinations, *Phys. Rev. B* **101**, 220202 (2020).
- [39] A. Teruya, A. Nakamura, T. Takeuchi, H. Harima, K. Uchima, M. Hedo, T. Nakama, and Y. Ōnuki, De haas–van alphen effect and fermi surface properties in nearly ferromagnet SrCo_2P_2 , *Journal of the Physical Society of Japan* **83**, 113702 (2014).
- [40] J. Mansart, P. Le Fèvre, F. m. c. Bertran, A. Forget, D. Colson, and V. Brouet, Influence of surface symmetry breaking on the magnetism, collapsing, and three-dimensional dispersion of the Co pnictides ACo_2As_2 ($A = \text{Ba}, \text{Sr}, \text{Ca}$), *Phys. Rev. B* **94**, 235147 (2016).
- [41] H. Mao and Z. Yin, Electronic structure and spin dynamics of ACo_2As_2 ($A = \text{Ba}, \text{Sr}, \text{Ca}$), *Phys. Rev. B* **98**, 115128 (2018).
- [42] K. Ali and K. Maiti, Emergent electronic structure of cafe_2as_2 , *Scientific Reports* **7**, 6298 (2017).
- [43] C. Liu, T. Kondo, N. Ni, A. D. Palczewski, A. Bostwick, G. D. Samolyuk, R. Khasanov, M. Shi, E. Rotenberg, S. L. Bud'ko, P. C. Canfield, and A. Kaminski, Three-to two-dimensional transition of the electronic structure in CaFe_2As_2 : A parent compound for an iron arsenic high-temperature superconductor, *Phys. Rev. Lett.* **102**, 167004 (2009).
- [44] J. Huang, Z. Wang, H. Pang, H. Wu, H. Cao, S.-K. Mo, A. Rustagi, A. F. Kemper, M. Wang, M. Yi, and R. J. Birgeneau, Flat-band-induced itinerant ferromagnetism in rbco_2se_2 , *Phys. Rev. B* **103**, 165105 (2021).

Supplementary Material of: ‘Flat band driven itinerant magnetism in the
Co-pnictides $(\text{La,Ca})\text{Co}_2(\text{As,P})_2$ ’

CONTENTS

A. DFT Calculation Details	2
B. Ferromagnetic solution CaCo_2As_2	4
C. DFT: surface state calculation of CaCo_2As_2 and LaCo_2P_2	5
D. ARPES	6
References	7

Appendix A: DFT Calculation Details

DFT calculations of the electronic band structure were carried out using the *Vienna Ab-initio Simulation Package* (VASP) software [1, 2] for the experimental structures available on Materials Project [3]. We chose the Perdew-Burke-Ernzenhof (PBE) implementation of the Generalized Gradient Approximation (GGA) for the exchange-correlation functional [4] together with Projector Augmented Wave (PAW) pseudo-potentials [5]. The k -point grid was adjusted to a Gamma-centered, regular Monkhorst-Pack point set of dimensions $13 \times 13 \times 13$ and the plane wave basis energy-cutoff was fixed to 600 eV. In order to accurately describe the d valence electrons, a series of DFT+ U calculations in the rotational-invariant implementation [6] were performed to fit the optimal value of the repulsive U parameter in the d subspace to reproduce the reported experimental magnetic moment [7, 8]. It was determined that $U = 1$ for AFM CaCo_2As_2 and $U = 1$ for FM LaCo_2P_2 , with resulting magnetic moments of $0.6\mu_B$ and $0.485\mu_B$ per atom, respectively. A Wannier function basis accurately describing the band structure around ± 1 eV from the Fermi level was constructed using Wannier90 [9]. Furthermore, we used the interpolated tight-binding Hamiltonian obtained in this basis to compute the Fermi surface and surface states using WannierTools [10].

Figures 1 and 2 show the DFT calculations of the bulk bands for the paramagnetic and magnetic ground states of CaCo_2As_2 and LaCo_2P_2 , respectively. The slab calculations are shown in Figure 5.

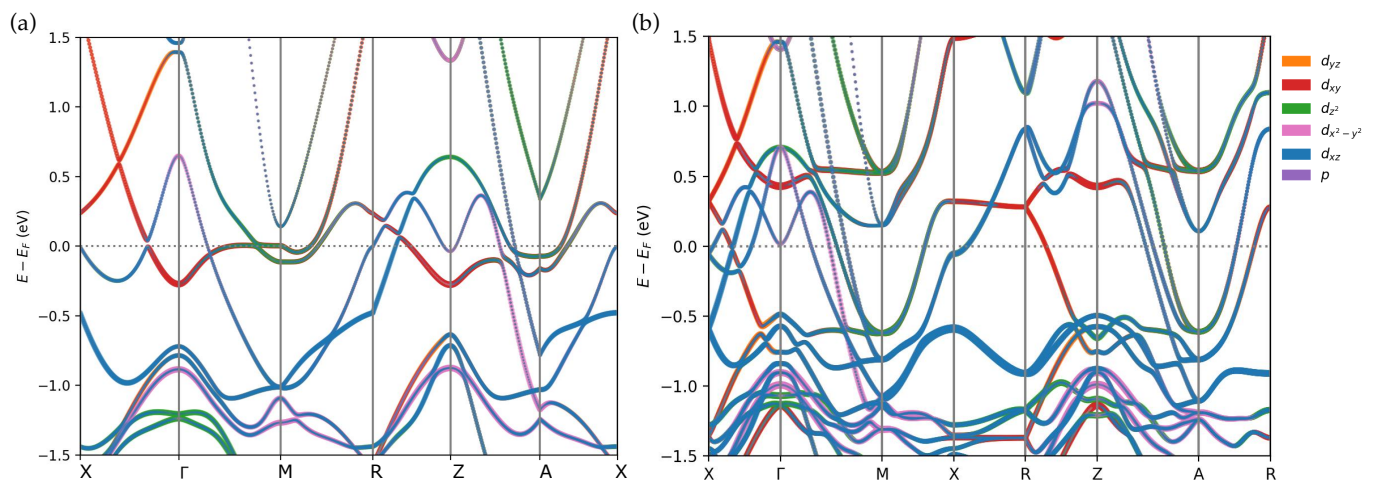


FIG. 1. Orbital resolved DFT calculation for CaCo_2As_2 for (a) PM and (b) AFM. The thickness encodes the weight of each atomic orbital component in the Bloch eigenstate.

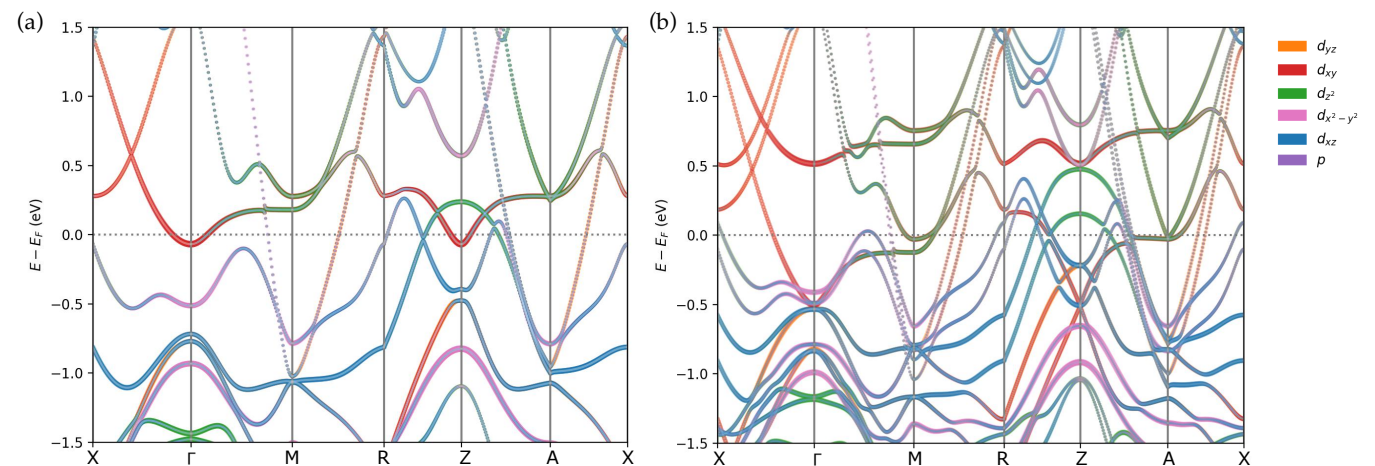


FIG. 2. Orbital resolved DFT calculation for LaCo_2P_2 for (a) PM and (b) FM. The thickness encodes the weight of each atomic orbital component in the Bloch eigenstate.

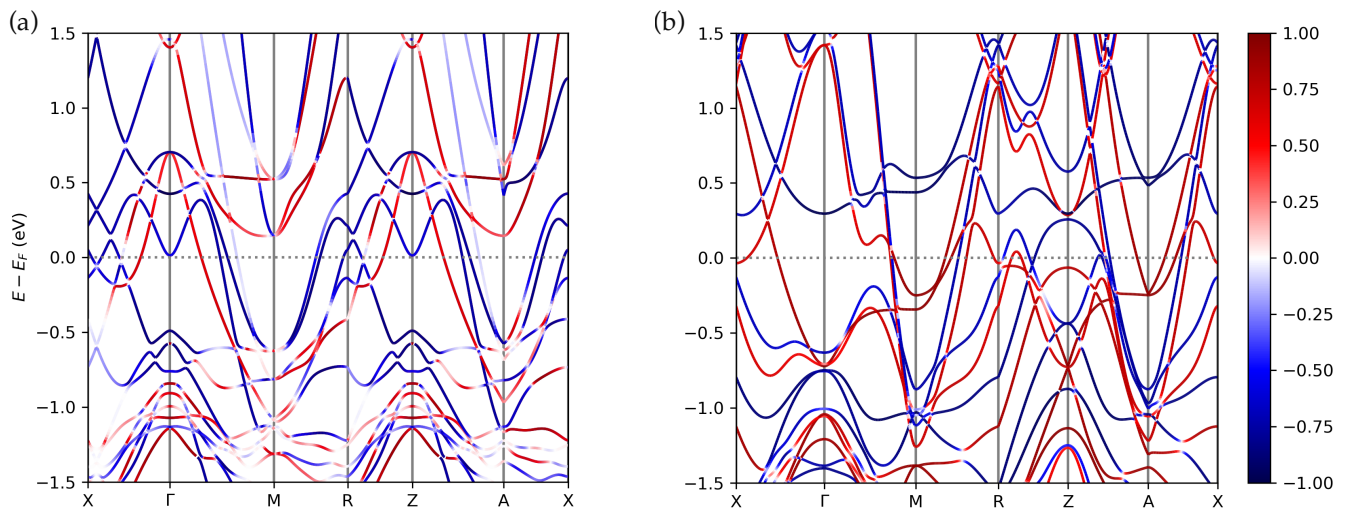


FIG. 3. Spin-projected DFT calculations colored according to the projection onto the magnetization axis. (a) S_z projection in AFM CaCo_2As_2 showing that there is no clear separation between spin-up and down bands and Kramers degeneracy. (b) S_x projection in FM LaCo_2P_2 where there is still good separation of the spin split bands except at points where spin-up and down bands hybridize due to SOC.

Orbital	CaCo_2As_2 (μ_B)	LaCo_2P_2 (μ_B)
s	0.00872	0.01393
p_y	-0.00384	-0.00422
p_z	0.00231	0.00264
p_x	-0.00143	-0.00422
d_{xy}	0.39144	0.62370
d_{yz}	0.03668	0.06977
d_{z^2}	0.12087	0.22284
d_{xz}	0.03263	0.06957
$d_{x^2-y^2}$	0.00066	0.01668

TABLE I. Contribution to the final magnetic momenta of the Co atoms separated by orbital. The values are computed from the expectation value of the σ_i (where $i = z, x$ for CaCo_2As_2 and LaCo_2P_2 , respectively) operators of the Kohn-Sham eigenstates projected onto the spherical harmonics and integrated up to the Fermi level.

Appendix B: Ferromagnetic solution CaCo_2As_2

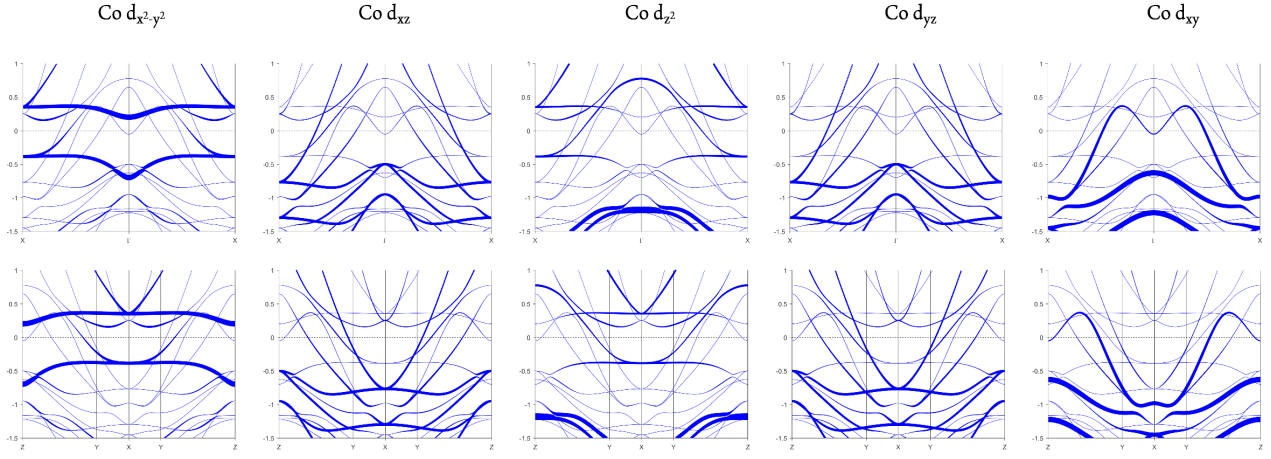


FIG. 4. Orbital resolved FM DFT calculation for CaCo_2As_2 . Note that the Co band with d_{xz} and d_{yz} character matches the band dispersion the experimental ‘ Λ ’ band.

Appendix C: DFT: surface state calculation of CaCo_2As_2 and LaCo_2P_2

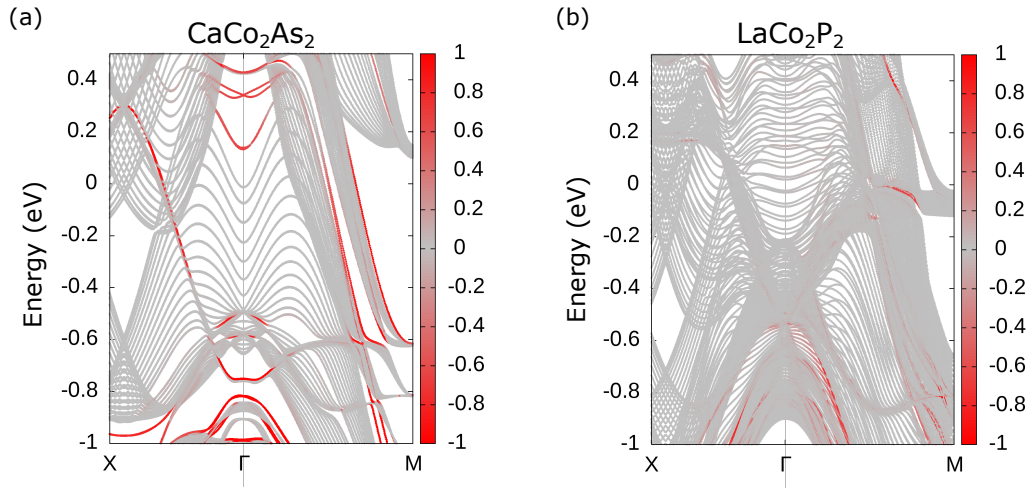


FIG. 5. Surface Bands calculation for (a) CaCo_2As_2 and (b) LaCo_2P_2 . The bands are computed using a slab with 15 cells in the tetragonal c axis direction using the Wannier tight-binding model. The color represents the weight of the eigenstates on the surface atoms computed from the eigenvectors of the Bloch Hamiltonian.

Appendix D: ARPES

Figure 6 shows a zoom of the panels of Figure 3 with higher resolution. In the main text, we discuss the presence of a flat band along the direction $\Gamma - M$ in CaCo_2As_2 for the paramagnetic phase (see Figure 1 (a)). Figure 7 shows the ARPES measurement taken with LV light and its corresponding Energy Distribution Curves (EDC) analysis. Panel (b) highlights the presence of a flat band in the EDC spectra.

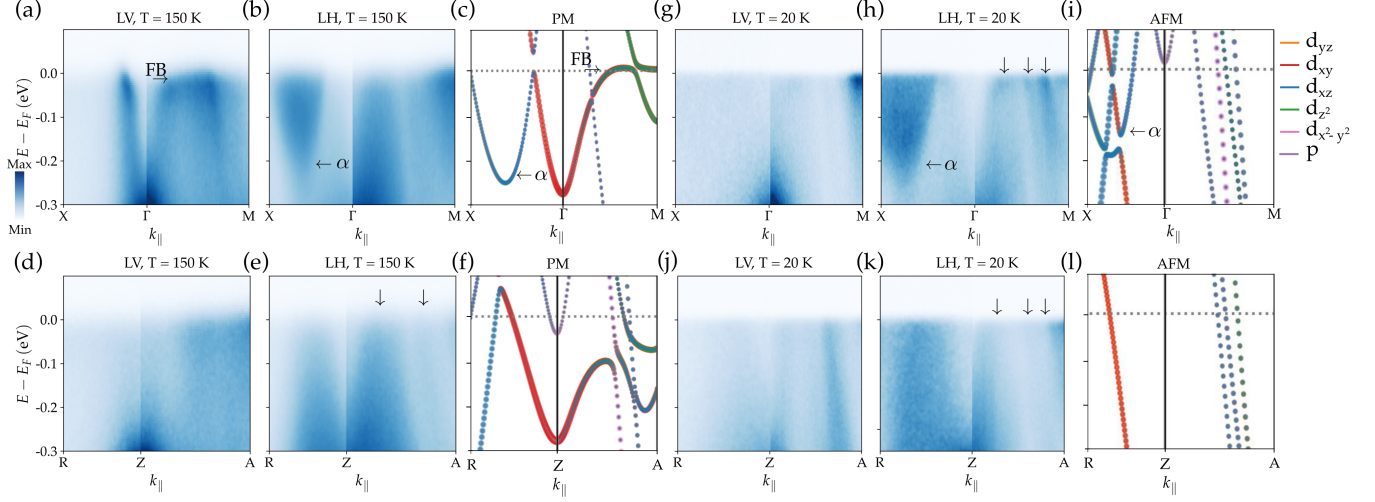


FIG. 6. Zoom panels of Figure 3 with binding energy axis $E - E_F = [0.3, 0.1]$ eV. (a-b) Electronic band dispersion of CaCo_2As_2 along the high symmetry lines $X - \Gamma - M$ taken with linear vertical (LV) and horizontal (LH) light, respectively, at $k_z = 0$ ($E_i=78$ eV), $T=150$ K. (c) Atomic orbital contribution DFT calculation of Co the d orbitals in the paramagnetic state at $k_z \simeq 0$. (d,e) Electronic energy bands along the high symmetry lines $R - Z - A$, $E_i=105$ eV. (f) Atomic orbital contribution DFT calculation of Co the d orbitals at $k_z=\pi$. (g-h) Band dispersion at low temperature, $T=10$ K and $k_z \simeq 0$. (i) Atomic orbital contribution DFT calculation, $k_z = 0$. (j-k) Band dispersion and (l) DFT calculation at $k_z = \pi$.

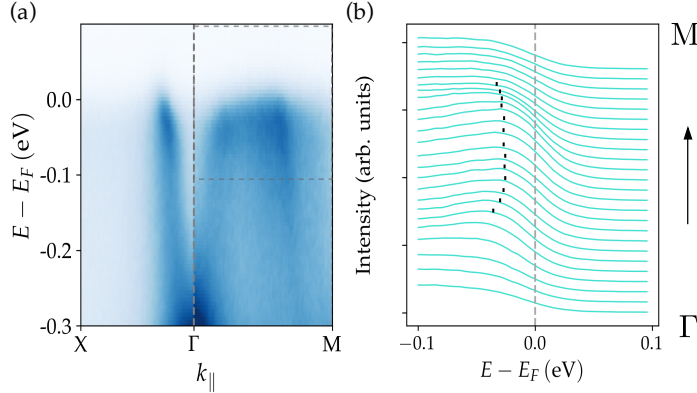


FIG. 7. (a) ARPES measurement taken with LV at $T = 150$ K CaCo_2As_2 . (b) EDC analysis of the square region of (a), highlighting the maximum of each EDC.

-
- [1] G. Kresse and J. Furthmüller, *Physical Review B* **54**, 11169 (1996), publisher: American Physical Society.
 - [2] G. Kresse and J. Hafner, *Physical Review B* **47**, 558 (1993), publisher: American Physical Society.
 - [3] A. Jain, S. P. Ong, G. Hautier, W. Chen, W. D. Richards, S. Dacek, S. Cholia, D. Gunter, D. Skinner, G. Ceder, and K. A. Persson, *APL Materials* **1**, 011002 (2013).
 - [4] J. P. Perdew, K. Burke, and M. Ernzerhof, *Physical Review Letters* **77**, 3865 (1996), publisher: American Physical Society.
 - [5] P. E. Blöchl, *Physical Review B* **50**, 17953 (1994), publisher: American Physical Society.
 - [6] S. L. Dudarev, G. A. Botton, S. Y. Savrasov, C. J. Humphreys, and A. P. Sutton, *Phys. Rev. B* **57**, 1505 (1998).
 - [7] B. Cheng, B. F. Hu, R. H. Yuan, T. Dong, A. F. Fang, Z. G. Chen, G. Xu, Y. G. Shi, P. Zheng, J. L. Luo, and N. L. Wang, *Phys. Rev. B* **85**, 144426 (2012).
 - [8] O. K. Forslund, D. Andreica, H. Ohta, M. Imai, C. Michioka, K. Yoshimura, M. Månsson, and J. Sugiyama, *Physica Scripta* **96**, 125864 (2021).
 - [9] A. A. Mostofi, J. R. Yates, G. Pizzi, Y.-S. Lee, I. Souza, D. Vanderbilt, and N. Marzari, *Computer Physics Communications* **185**, 2309 (2014).
 - [10] Q. Wu, S. Zhang, H.-F. Song, M. Troyer, and A. A. Soluyanov, *Computer Physics Communications* **224**, 405 (2018).